Title

Controlled defibrillation of rice straw cellulose and self-assembly of cellulose nanofibrils into highly crystalline fibrous materials

Journal

RSC Advances, 3(30)

ISSN

2046-2069

Authors

Jiang, F
Han, S
Hsieh, YL

Publication Date

2013-08-14

DOI

10.1039/c3ra41646a

Peer reviewed

RSC Advances

RSC Publishing

PAPER

Controlled defibrillation of rice straw cellulose and self-assembly of cellulose nanofibrils into highly crystalline fibrous materials†

Cite this: *RSC Advances*, 2013, **3**, 12366

Feng Jiang, Siyuan Han and You-Lo Hsieh*

Coupled chemical–mechanical defibrillation and self-assembly processes have been successfully established for creating super-fine (125–497 nm wide) highly crystalline (63.2–71.5% CrI) cellulose Iβ fibrous materials from rice straw cellulose. Under the optimized TEMPO mediated oxidation with 5 mmol g^{-1} NaClO/cellulose followed by 30 min mechanical blending, highly uniform (2.09 nm wide, 1.52 nm thick, up to 1 μm long) cellulose nanofibrils (CNFs) were efficiently derived at an impressive 96.8% yield and contained 1.29 mmol surface carboxyls per g of cellulose or 0.21 COOH/anhydroglucose (AG), representing 70.9% surface C6 primary hydroxyl to carboxyl conversion. Rapid freezing of aqueous CNF suspensions in liquid nitrogen and freeze-drying induced self-assembly of these nanofibrils into white fluffy fibrous materials *via* ice-crystal templating. The self-assembled fiber morphologies showed a strong dependence on CNF morphologies and extent of surface carboxylation. CNFs with 37.3% conversion of surface carboxyls assembled into 125 nm wide fibers, whereas wider fibers (327 nm and 497 nm) were assembled from the smaller CNFs and more carboxylated (51.5% and 70.9%, respectively) surfaces. This robust defibrillation–assembly approach offers new versatile and scalable alternatives to fabricate super-fine cellulose fibers with a highly crystalline cellulose Iβ structure from the by-product of the largest cereal crop in the world.

Received 5th January 2013,
Accepted 20th May 2013

DOI: 10.1039/c3ra41646a

www.rsc.org/advances

Introduction

Cellulose, the most abundant natural polymer, consists of highly stereo-regular and hydrogen bonded β(1,4)-glycosidic linked D-glucose chains organized in hierarchical structures of nanofibrils (3–4 nm), microfibers (10–30 nm) and macrofibers (over hundreds of nm and microns).[1,2] The highly crystalline cellulose nanofibrils have been reported to exhibit exceptional properties such as superior elastic modulus of 150 GPa,[3] low thermal expansion coefficient of 10^{-7} K^{-1} in the axial direction[4] and high specific surface areas and chemical reactivities in addition to their nanoscale dimensions.[5–7]

The elementary cellulose nanocrystals (CNCs) and nanofibrils (CNFs) have been isolated from various native sources by overcoming the inter-fibrillar hydrogen bonds and/or breaking the less crystalline chains *via* chemical reactions such as acid hydrolysis,[8–10] 2,2,6,6-tetramethylpyperidine-1-oxyl (TEMPO) mediated oxidation,[11,12] biochemical enzymatic hydrolysis,[13] mechanical defibrillation[14,15] or a combination of the above. Sulfuric acid hydrolysis liberates the most uniform (3–5 nm wide, 100–200 nm long from wood)[8,16] and often highly crystalline (54–91%)[7,17] rod-like CNCs, but at yields usually less than 30%.[18] Mechanical defibrillation, on the other hand, improved the yield to nearly 100% but also gave less uniform microfibrillated fibrils with widths ranging to over 100 nm, while requiring high input of energies (700–1400 MJ kg^{-1}).[19] TEMPO mediated oxidation alone led to oxidized cellulose fibers in similar macroscopic morphology as the original cellulose, yielding very few nanofibrils.[11,20] The CNF yields from TEMPO oxidized cellulose could be improved to over 90% by further mechanically processing such as blending,[21] magnetic stirring,[22] ultrasonication[12] and alternative blending and ultrasonication.[23] Common household blender has shown to defibrillate wood pulp[15] and alkaline treated banana rachis.[24]

Nanocellulose has been isolated mostly from wood,[9] bacterial cellulose,[25] marine animals[26] and fiber crops such as cotton,[27] and increasingly from agricultural crop residues such as rice straw.[17,28] As a readily available byproduct of the world largest cereal crop and with relatively high cellulose contents of approaching 40%,[17] rice straw is among the most significant non-wood cellulose sources. Deriving nanocellulose from rice straw presents excellent prospect for this under-utilized and globally available crop byproduct. Sulfuric acid hydrolysis (64 wt%, 8.75 mL g^{-1} acid-to-cellulose ratio, 45 °C,

Fiber and Polymer Science, University of California, Davis, CA95616, USA. E-mail: ylhsieh@ucdavis.edu; Fax: +1 530 752 7584; Tel: +1 530 752 0843

† Electronic supplementary information (ESI) available: Validation of Henry equation and the Huckel approximation for zeta potential measurement, conductometric titration curve of TEMPO oxidized cellulose at 5 mmol NaClO g^{-1} of cellulose without adding HCl, optical microscopic images of blended CFs, crystallite dimensions and calculated surface C6 primary hydroxyls, DTGA curves of rice straw cellulose and assembled CNFs. See DOI: 10.1039/c3ra41646a

45 min) of rice straw cellulose has however yielded only 6% CNCs.[17] Shortening the hydrolysis time to 15 min increased the yield to 17%,[29] a nearly three-fold increase, but the resulting CNCs were more heterogeneous in shapes and bimodally distributed in dimensions. Either mechanical blending or TEMPO mediated oxidation alone showed indifferent improvement of CNF yield to 12% and 20%, respectively.[29] Intriguingly, both rice straw CNCs[17] and CNFs[29] have shown to form submicrometer sized fibers from liquid nitrogen freezing and freeze-drying processes.

This study was aimed to optimize CNF isolation from rice straw by coupling TEMPO mediated oxidation and mechanical blending and to investigate CNF self-assembling behavior and relationship to their structures. TEMPO mediated oxidation was conducted at varying primary oxidant NaClO quantities from 1.5 to 10 mmol per g of rice straw cellulose or 0.24 to 1.62 NaClO/anhydroglucose (AG) molar ratios. TEMPO oxidized rice straw cellulose was defibrillated for different time intervals using a common household blender. Suspension appearance, optical microscopy and yields were observed to determine the optimal conditions of the combined TEMPO-mechanical process, *i.e.*, the minimal primary oxidant and mechanical defibrillation levels necessary for optimal yield and quality of CNFs. The isolated CNFs were characterized by their surface properties and morphologies and their self-assembling behavior into fibrous materials *via* rapid freezing and freeze-drying was closely followed in terms of the fiber morphologies, crystalline and chemical structures and thermal stability and correlated to CNF surface chemistry and morphologies.

Experimental

Materials

Pure cellulose was isolated from rice straw (Calrose variety) by a three-step process of 2 : 1 v/v toluene/ethanol extraction, acidified $NaClO_2$ dissolution of lignin (1.4%, 70 °C, 5 h), and alkaline dissolution of hemicellulose and silica (5% KOH, 90 °C for 2 h), to a 36% yield.[17] Hydrochloric acid (HCl, 1N, Certified, Fisher Scientific), sodium hydroxide (NaOH, 1N, Certified, Fisher Scientific), sodium hypochlorite (NaClO, 11.9%, reagent grade, Sigma-Aldrich), 2,2,6,6-tetramethylpyperidine-1-oxyl (TEMPO, 99.9%, Sigma-Aldrich), sodium bromide (NaBr, BioXtra, 99.6%, Sigma-Aldrich) were used as received without further purification. All water used was purified by Milli-Q plus water purification system (Millipore Corporate, Billerica, MA).

TEMPO mediated oxidation and mechanical defibrillation of rice straw cellulose

TEMPO mediated oxidation was conducted at four levels following a previously reported procedure.[12,30] Rice straw cellulose (1.0 g) was added to 100 mL water and mixed with a magnetic stirrer for 5 min, then 2 mL of an aqueous mixture of TEMPO (0.016 g) and sodium bromide (0.1 g) was added and stirred for another 5 min. Oxidation reaction was initiated by adding 11.9% NaClO drop-wise until reaching specific NaClO concentrations of 1.5, 3, 5 and 10 mmol per gram of cellulose. The pH decreased as oxidation proceeded and was adjusted to 10 ± 0.2 with 0.5 M NaOH. The oxidation reaction ended when no acid was produced or pH ceased to lower, and the reaction time was recorded. The pH was then adjusted to 7 with 0.5 M HCl. The suspension was centrifuged at 5000 rpm for 15 min and dialyzed against water for several days. The white turbid suspension after dialysis was recovered and designated as TEMPO oxidized cellulose fibers CF1.5, CF3, CF5 and CF10 for samples oxidized with 1.5, 3, 5 and 10 mmol g^{-1} NaClO/cellulose, respectively.

100 ml of 0.1 wt% CF suspension was transferred to a 2 L blender beaker and blended at 37 000 rpm (Vitamix 5200) for specific lengths of time, *i.e.* 1 to 60 min for CF1.5 and CF3 and 1 to 30 min for CF5. The blended suspensions were allowed to settle at 4 °C for 24 h and imaged. Each suspension was centrifuged at 4500 rpm for 15 min to separate and filter (Whatman 541) the CNF containing supernatant from the precipitate where larger cellulose fragments were collected for optical imaging. The yields of CNFs were calculated based on their weights over the starting oxidized cellulose and reported as percentages. CNFs from the longest blending time, *i.e.* 60 min for CF1.5 and CF3, 30 min for CF5, were designated as CNF1.5, CNF3 and CNF5, respectively, and characterized.

Self-assembly of fibrous cellulosic materials

Sub-micron fibrous cellulosic materials were assembled from 0.1 wt% CNF aqueous suspensions *via* a rapid freezing and freeze-drying process. Typically, CNFs (20 mL) was placed in 50 mL centrifuge tubes, quickly immersed into liquid nitrogen and lyophilized at −50 °C in a freeze-drier (FreeZone 1.0 L Benchtop Freeze Dry System, Labconco, Kansas City, MO).

Characterization

Conductometric titration. Certain amount of 1 N HCl was added to 50 mL of 0.1 wt% CF suspension to protonate all the carboxyl groups, then titrated with 0.01 M NaOH solution. The conductivity values were recorded using OAKTON pH/Con 510 series meter. The surface charge (σ, in mmol g^{-1} of cellulose) was determined from equation,

$$\sigma = \frac{cv}{m} = \frac{c(v_2 - v_1)}{m} \quad (1)$$

where c is the NaOH concentration (in M), m is the CF mass in the suspension (in g), and v_1 and v_2 are NaOH volumes (in mL) used from neutralizing the added HCl and carboxylic acid on the CFs, respectively.

Zeta potential measurement. Zeta potential (ζ) of 0.1 wt% aqueous CNF suspension was measured using a Zetasizer Nano S90 (Malvern Instrument) without adjusting ionic strength. The ζ value was calculated from the electrophoretic mobility using Henry equation and Huckel approximation[31] as validated in the ESI.† Three measurements were conducted for each suspension and the mean and standard deviation were reported.

Optical microscopy. The CF precipitates after CNF isolation were diluted by adding 20 mL water, stirred, and observed

under a Leica DM2500 optical microscope equipped with cross polarized filter.

Atomic force microscopy (AFM). CNF suspension (10 μL, 0.002 wt%) was deposited onto a freshly cleaved mica surface, air-dried, scanned (Asylum-Research MFP-3D) in air under ambient condition using tapping mode with OMCL-AC160TS standard silicon probes. The scan rate was set to 1 Hz and image resolution is 512 × 512 pixels. The height images and profiles were processed with Igor Pro 6.21 loaded with MFP3D 090909 + 1409, and the average thickness was determined from *ca.* 200 individual nanofibrils. For CNF1.5 and CNF3, only smaller fibrils with thickness less than 5 nm were determined for comparison.

Transmission electron microscopy (TEM). CNF suspension (8 μl, 0.01 wt%) was deposited onto glow-discharged carbon-coated TEM grids (300-mesh copper, formvar-carbon, Ted Pella Inc., Redding, CA) with the excess liquid being removed by blotting with a filter paper after 10 min. The specimens were then negatively stained with 2% uranyl acetate solution for 5 min, blotted with a filter paper to remove excess staining solution and allowed to dry under the ambient condition. The samples were observed using a Philip CM12 transmission electron microscope operated at a 100 kV accelerating voltage. The width of CNFs was measured from *ca.* 200 individual nanofibrils using an image analyzer (ImageJ, NIH, USA). Again, a cut-off value of 5 nm was used for CNF1.5 and CNF3 to exclude the larger fibrils.

X-ray diffraction (XRD). XRD spectra for pure rice cellulose and freeze-dried CNFs were collected on a Scintag XDS 2000 powder diffractometer using a Ni-filtered Cu-Kα radiation (λ = 1.5406 Å) at an anode voltage of 45 kV and a current of 40 mA. Freeze-dried samples were compressed between two glass slides into flat sheets with around 1 mm thickness. Diffractograms were recorded from 5° to 40° at a scan rate of 2° min^{-1}. Crystallinity index (CrI) was calculated from the intensity of the 200 peak (I_{200}, 2θ = 22.6°) and the intensity minimum between the peaks at 200 and 110 (I_{am}, 2θ = 18.7°) by using the empirical equation,[32]

$$\mathrm{CrI} = \frac{I_{200} - I_{\mathrm{am}}}{I_{200}} \times 100 \quad (2)$$

The crystallite dimensions of these samples were calculated using Scherrer equation,[33]

$$D_{hkl} = \frac{0.9\lambda}{\beta_{1/2}\cos\theta} \quad (3)$$

where D_{hkl} is the crystallite dimension in the direction normal to the *hkl* lattice planes, λ is the X-ray radiation wavelength (1.5406 Å), $\beta_{1/2}$ is the full width at half-maximum of the diffraction peak, and θ is the corresponding Bragg angle. $\beta_{1/2}$ was determined from Voigt profile fits of the diffraction peaks calculated with PeakFit (v4.12, Systat Software, Inc.). The primary C6 hydroxyl groups on cellulose crystal surfaces (mol per mol of AG, OH/AG) were determined using equation,[34]

$$\text{Surface primary hydroxyls} = \frac{(D/0.61 + D/0.53)}{(D/0.61 + 1) \times (D/0.53 + 1)} \quad (4)$$

where 0.61 nm, 0.53 nm and D are the d-spacings and average crystallite dimension of the $1\bar{1}0$ and 110 crystallographic planes of cellulose I structures, respectively.

Fourier transform infrared spectroscopy (FTIR). FTIR spectra of freeze-dried rice straw cellulose and CNFs in KBr pellets (1 : 100, w/w) were collected using a Thermo Nicolet 6700 spectrometer. The spectra were collected at ambient conditions in the transmittance mode from an accumulation of 128 scans at a 4 cm^{-1} resolution over the regions of 4000–400 cm^{-1}.

Scanning electron microscopy (SEM). Freeze-dried CNFs were mounted with conductive carbon tape, sputter coated with gold and imaged by a field emission scanning electron microscope (FE-SEM) (XL 30-SFEG, FEI/Philips, USA) at a 5-mm working distance and 5-kV accelerating voltage. The diameters of freeze-dried CNFs were calculated from measurements of over 100 individual fibers using an image analyzer (ImageJ, NIH, USA).

Thermogravimetric analysis (TGA). TGA analyses of rice straw cellulose and freeze-dried CNFs were performed on a TGA-50 thermogravimetric analyzer (Shimadzu, Japan). Each sample (5 mg) was heated at 10 °C min^{-1} from 25 °C to 500 °C under purging N_2 (50 mL min^{-1}).

Results and discussion

TEMPO-mediated oxidation of rice straw cellulose

Pure cellulose isolated from rice straw was oxidized *via* TEMPO/NaBr/NaClO oxidation at four primary oxidant NaClO levels of 1.5, 3, 5 and 10 mmol NaClO per g of cellulose or 0.24, 0.49, 0.81 and 1.62 mol NaClO per mol of anhydroglucose (AG) to convert the C6 primary hydroxyls to carboxyls. The charges associated with the carboxyls of TEMPO oxidized cellulose fibers (CFs) were measured by conductometric titration whose curves showed parabolic-shape relationships with NaOH amount at all four NaClO levels (Fig. 1a). The initial decreases in conductivity reflected the neutralization of NaOH with added HCl and were unrelated to the charge nature of CFs. Upon complete neutralization, the conductivity plateaued where NaOH consumption was associated with the weak carboxylic acid on the oxidized CFs. A steep increasing trend following the plateau indicated the accumulated NaOH in the titrand. The charges associated with the carboxyls were calculated from NaOH consumed in the plateau regions to be 0.59, 0.92, 1.29 and 1.68 mmol C6 carboxyls per g of cellulose, or 0.10, 0.15, 0.21 and 0.27 mol C6 carboxyls per mol of AG (COOH/AG) for CF1.5, CF3, CF5 and CF10, respectively (inset, Fig. 1a). A highly positive linear relationship was observed between hydroxyl to carboxyl conversion at NaClO amounts of 1.5 to 5 mmol g^{-1} NaClO/cellulose at a very high correlation coefficient R^2 = 0.9997 (Fig. 1b).

Under basic reaction condition (pH 10), the newly formed carboxyl groups reacted with NaOH to sodium carboxylates. In all cases, the added HCl protonates the sodium carboxylate

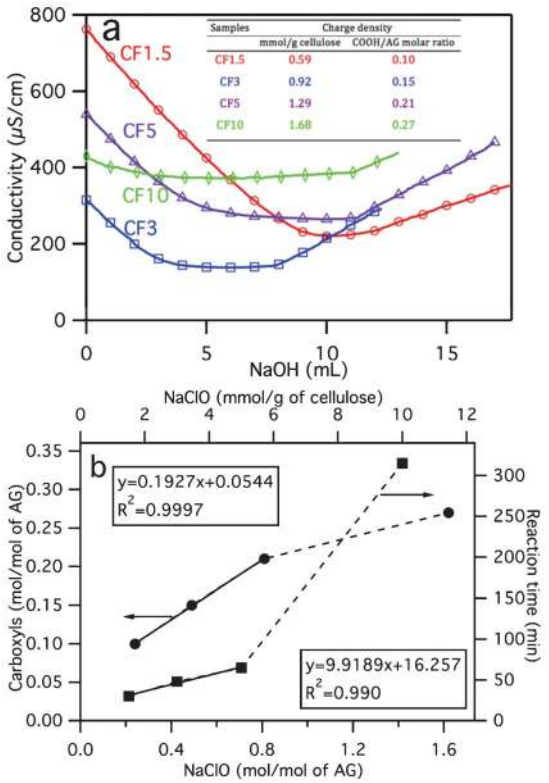

Fig. 1 TEMPO oxidized cellulose: (a) conductometric titration at: 1.5 mmol (○), 3 mmol (□), 5 mmol (△) and 10 mmol (◇) NaClO/g of cellulose (inset: charges calculated according to eqn (1)); (b) charge and reaction time *versus* NaClO amount (insets: linear regression fitting equations and correlation coefficients).

into carboxylic acid, thus the calculated surface charge densities represent all the surface carboxyls, either in acid or salt forms. To determine the proportion of sodium carboxylate salts on CF5, conductometric titration was conducted without HCl (Fig. S1 in the ESI†). In contrast to titration with added HCl (Fig. 1a), the initial decrease in conductivity disappeared from the titration curve without HCl, showing only two stages of increasing slopes, representing neutralization of the carboxylic acid and accumulation of added NaOH, respectively. The amount of carboxylic acid was determined to be 0.178 mmol g^{-1} of cellulose from the NaOH consumed by neutralization of carboxylic acid, *i.e.* 86% of the carboxylic groups are in the sodium salt form based on the 1.29 mmol total carboxyls per g of cellulose.

Similar to the positive linear relationship between surface charges and NaClO quantities, the lengths of time to reach complete oxidation also increased linearly from 30 min to 65 min with increasing NaClO from 1.5 to 5 mmol g^{-1} NaClO/cellulose with a high correlation coefficient R^2 = 0.990 (Fig. 1b). These times taken to reach complete oxidation of rice straw cellulose were relatively fast, even at the ambient temperature, achieving a high charge of 1.29 mmol g^{-1} of cellulose at 5 mmol g^{-1} NaClO/cellulose in 65 min. TEMPO mediated oxidation is a heterogeneous reaction that takes place primarily in the amorphous regions and on crystal surfaces that are accessible to the oxidizing reagents. These linear relationships of charge or reaction time with NaClO levels suggest the accessibility and diffusion of the active oxidizing agent, N-oxoammonium ion or TEMPO nitroxyl radical, in rice straw cellulose are similar in the 1.5–5 mmol g^{-1} NaClO/cellulose or 0.24–0.81 NaClO/AG molar ratio range. On the other hand, oxidation at a higher NaClO level of 10 mmol g^{-1} NaClO/cellulose, or 1.62 NaClO/AG, produced a higher surface charge of 1.68 mmol g^{-1} of cellulose, or 0.27 COOH/AG, but at a significantly longer reaction time of 315 min, both deviating from the linear relationships observed in 1.5–5 mmol g^{-1} NaClO/cellulose region (Fig. 1b). Since the reaction time reflects accessibility to the C6 hydroxyls, the deviation at the highest 10 mmol g^{-1} NaClO/cellulose level suggests retarded accessibility of the oxidants, possibly by the crystalline domains. Disproportionately increased reaction time from 40–45 min to 115–130 min was also reported in TEMPO oxidation of hardwood kraft pulp at 3.8–5 mmol g^{-1} NaClO/cellulose.[22] Comparing to kraft pulp oxidized at the same 5 mmol g^{-1} NaClO/cellulose level, the 65 min reaction time was significantly shorter for rice straw cellulose than the 130 min for kraft pulp, indicating greater accessibility of TEMPO nitroxyl radicals in rice straw cellulose.

In TEMPO/NaBr/NaClO oxidation, both TEMPO and NaBr serve as catalysts. NaBr is oxidized by primary oxidant NaClO to a much stronger secondary oxidant hypobromite, which then oxidizes TEMPO to N-oxoammonium ion. Upon oxidizing cellulose C6 hydroxyl, N-oxoammonium ion is reduced to hydroxylamine then oxidized back to TEMPO nitroxyl radical. In this process, one equivalent of the primary oxidant NaClO is consumed to convert each primary hydroxyl group to aldehyde, while another equivalent is needed to convert each aldehyde to carboxyl. Considering a 2 NaClO/AG molar ratio to theoretically convert primary hydroxyls to carboxyls, the oxidant quantity needed to convert those on amorphous cellulose chains and the crystal surfaces are expected be considerably less than the total AG in cellulose. Using the carboxyl values determined by conductometric titration, the NaClO to surface carboxyls ratios are 2.4, 3.3, 3.9 and 6 at 1.5, 3, 5 and 10 mmol g^{-1} NaClO/cellulose, respectively, all higher than the theoretical 2 NaClO/AG molar ratio and increasing with higher oxidant levels. These excess and increasing consumption of NaClO in TEMPO oxidation of rice straw cellulose at higher primary oxidant levels is possibly due to the less efficient access of oxidants to the remaining primary hydroxyls and aldehydes on the crystalline fibril surfaces.

Mechanical defibrillation of TEMPO oxidized rice straw cellulose

The oxidized rice straw cellulose suspensions were then subject to mechanical blending at 37 000 rpm for varying time intervals, then left settle at 4 °C for 24 h. Without blending, oxidized cellulose fibers settled as white layers at the bottom of suspensions (0 min vials, Fig. 2d–f), indicating CFs to be mainly micrometer wide fibers. With blending, the layers became less opaque and more diffused into the rest of suspension. For CF1.5 and CF3, the diffused volume expanded with longer blending times (from left to right, Fig. 2d,e), showing increasing defibrillation into smaller fibrils that remained suspended after 24 h. Still, some precipitates were

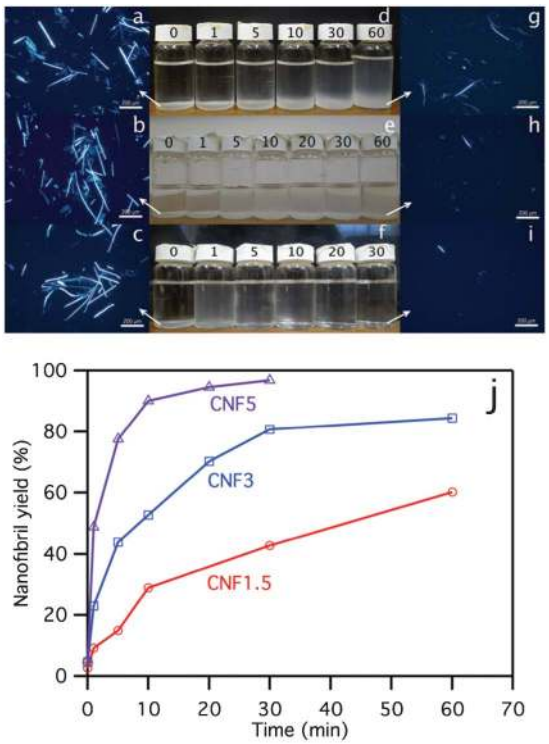

Fig. 2 TEMPO oxidized rice straw cellulose blended for varying lengths of time (min indicated): optical microscopic images under cross polarizers of the precipitates from original (a–c) and most blended (g–i), bar = 200 μm; photographs of 0.1% aqueous suspensions of CNF1.5 (d), CNF3 (e) and CNF5 (f); (j) yields of CNF1.5 (○), CNF3 (□) and CNF5 (Δ).

observed in CF1.5 and CF3 after 60 min, signs of incomplete defibrillation. At the optimal 5 mmol g^{-1} NaClO/cellulose or 0.81 NaClO/AG level (CF5, Fig. 2f), the suspension became translucent with little precipitate after blending for only 1 min, then even more transparent with longer blending of 5 and 10 min. Complete transparent suspension was observed after 20 min of blending, indicating most of the oxidized cellulose fibers have been defibrillated into nanofibrils. The suspensions were centrifuged to separate CNF-containing supernatants from the precipitates that were collected and redispersed in water and imaged under an optical microscope. Under cross polarizers, all precipitates from the original oxidized cellulose appeared to be mostly 5 μm wide and 100–500 μm long crystalline rod-like fibers, irrespective of the oxidant levels (Fig. 2a–c). Following the longest mechanical blending (60 min for CF1.5 and CF3, 30 min for CF5), few rods were observed in CF1.5, but very few and much shorter fibers were found in the precipitates of the more blended CF3 and CF5 (Fig. 2g–i). Overall, longer blending times led to more extensive defibrillation as expected and supported by optical microscopic observation of fibers in the precipitates (Fig. S2–4 in ESI†).

Each CNF-containing supernatant was centrifuged and filtered, then concentrated to determine CNF yield gravimetrically. TEMPO oxidation alone, *i.e.* with no blending, was capable of liberating small amounts of CNFs at 2.6%, 4.6% and 5.3% for CF1.5, CF3 and CF5, respectively (Fig. 2j). The

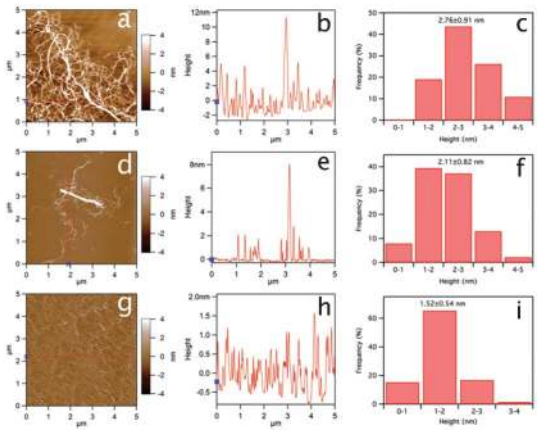

Fig. 3 AFM height images (a,d,g), height profiles (b,e,h) and height distribution (c,f,i) of TEMPO oxidized and mechanically defibrillated CNFs: (a–c) CNF1.5; (d–f) CNF3; (g–i) CNF5.

CNF yields increased with blending at all three oxidized levels. With only 10 min of blending, CNF yields increased drastically to 28.9%, 52.8% and 90.1% for CF1.5, CF3 and CF5, respectively. Blending for 60 min raised CNF yields further to 60.3% and 84.5% for CF1.5 and CF3, respectively. For CF5, a maximal 96.8% yield of CNFs was reached after 30 min blending, 14.6% and 60.5% higher than the highest yielding CF3 and CF1.5, respectively, at half of the blending time. At a higher degree of oxidation, *i.e.*, with 5 mmol g^{-1} NaClO/cellulose or 0.81 NaClO/AG molar ratio, CNF yields were more efficiently optimized by mechanical defibrillation.

Morphologies and charge nature of cellulose nanofibrils

The AFM height images of CNF1.5 and CNF3 showed heterogeneous morphologies of both thin and thick nanofibrils (Fig. 3a,d). CNF1.5 nanofibrils were several micrometers long whereas CNF3 were shorter, around 1–2 μm. Most CNF1.5 nanofibrils were 2–5 nm thick, averaging at 2.76 ± 0.91 nm (Fig. 3c), with few approaching 12 nm (Fig. 3b) whereas most CNF3 nanofibrils were 1–4 nm thick, averaging at 2.11 ± 0.82 nm (Fig. 3f) and 8 nm in one case (Fig. 3e). Most uniform nanofibril dimensions were observed for CNF5 with an average thickness of 1.52 ± 0.54 nm (Fig. 3h,i) and lengths up to 1 μm (Fig. 3g). The continuously decreased thickness with increased oxidation extent manifests that higher oxidation leads to more thorough separation of cellulose nanofibrils with the lateral dimensions of CNF5 approaching multiples of cellulose unit cell dimensions.

TEM images showed individual CNF1.5 and CNF3 nanofibrils to be 2 to 5 nm wide (Fig. 4a,c) and averagely 3.43 ± 0.60 and 2.86 ± 0.51 nm wide (Fig. 4b,d), respectively. The widths of CNF1.5 and CNF3 were approximately 24 and 36% higher than their thickness values determined from AFM height images. Additionally, 30–50 nm wide CNFs were also observed for both CNF1.5 and CNF3, possibly the less defibrillated CNFs as observed in AFM or from association of fine nanofibrils during drying in TEM sample preparation. Again, TEM images of CNF5 showed the most uniform nanofibrils, averaging 2.09 ± 0.44 nm wide (Fig. 4e,f), approximately 38% higher than its

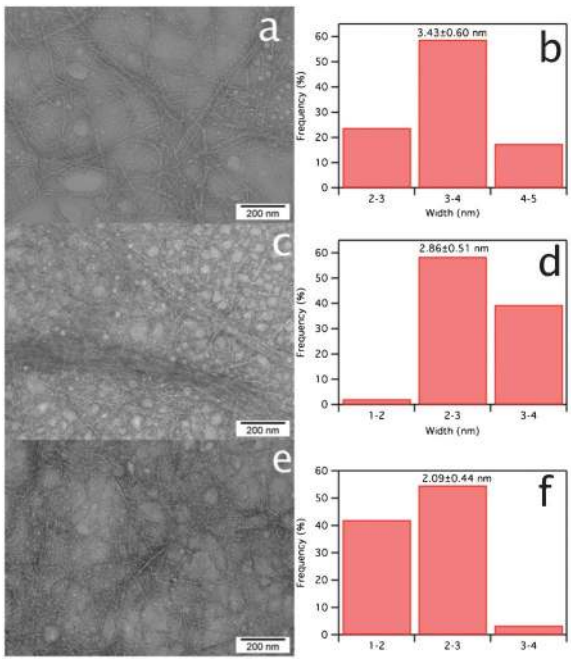

Fig. 4 TEM images (a,c,e) and width distribution (b,d,f) of TEMPO oxidized and mechanically defibrillated CNFs: (a,b) CNF1.5; (c,d) CNF3; (e,f) CNF5.

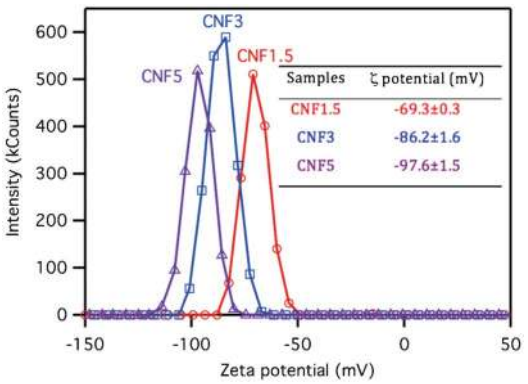

Fig. 5 Zeta potential of CNF1.5 (○), CNF3 (□) and CNF5 (△).

thickness. The 1.24 to 1.38 width-to-thickness ratios indicate the anisotropic lateral dimensions of these CNFs, possibly due to the differential intersheet and intrasheet bonding strengths involving hydrogen bonding and van der Waals interactions.[35] Intrasheet bondings include additional interchain hydrogen bonding and van der Waals interactions and have been reported to be about 8 times stronger than the intersheet bondings.[36] Besides, all observed lateral dimensions of CNFs are similar or smaller than the crystallite dimension (3.51 nm) of rice straw cellulose,[29] indicating the occurrence of both intersheet delamination and intrasheet hydrogen bonding cleavage under the combined TEMPO oxidation and mechanical blending process. The decreased lateral dimension with increased oxidation extent is consistent with the cleavage of inter-chain and intrasheet hydrogen bonds facilitated by the introduced carboxyl groups.

Both AFM and TEM images of CNFs revealed the nanofibril morphologies to be closely associated with the NaClO oxidant levels. Higher hydroxyl to carboxyl conversions afforded at higher oxidant levels enable more effective mechanical defibrillation of the oxidized cellulose yielding more uniform nanofibrils. Cellulose nanofibrils that are around 2 nm wide and up to 1 μm long were mechanically defibrillated from oxidized rice straw cellulose with the 1.29 mmol g^{-1} cellulose surface charge. Combining the very impressive 96.8% yield, TEMPO/NaBr/NaClO oxidation with 5 mmol g^{-1} NaClO/cellulose or 0.81 NaClO/AG molar ratio and 30 min mechanical blending is the optimal condition in yielding 2 nm wide and one micrometer long nanofibrils from rice straw cellulose. The lateral dimensions (1–2 nm) of CNF5 are remarkably thinner than those obtained from wood pulp cellulose (3–5 nm) following similar TEMPO oxidation and mechanical defibrillation procedures.[21,22,37] The high yield together with the significantly shorter reaction time discussed earlier clearly shows rice straw cellulose to be more easily defibrillated into nanofibrils than wood pulp. Although finer 1.38 nm CNF has been reported from TEMPO oxidation and sonication of wood pulp,[38] the 1 g rice straw cellulose quantity processed is significantly higher than the 0.012 g for wood pulp, making scale-up production of rice straw CNFs more feasible. The ultra-fine CNF quality and high quantity production indicate rice straw cellulose to be a highly viable and energy-efficient source for cellulose nanofibrils.

CNFs from the most extensive blending, *i.e.* 60 min for CNF1.5 and CNF3, 30 min for CNF5, all had narrowly distributed and negative ζ values that peaked at −69.3, −86.2 and −97.6 mV, respectively (Fig. 5). The increasing negative zeta potential values of CNFs with increasing primary oxidant NaClO levels follow the same trend as their surface charges. The more highly negative zeta potential values manifest the more highly converted surface C6 primary hydroxyls to carboxyls that are mostly in the charged sodium salt form as discussed earlier.

Self-assembly of cellulose fibrous materials

Upon rapid freezing the dilute (0.1 wt%) aqueous CNF suspensions in liquid nitrogen followed by freeze-drying, all three CNFs assembled into white fluffy fibrous mass. SEM of freeze-dried CNF1.5 showed self-assembled fibers to be very fine and curvy with 125 (±33) nm average diameter (Fig. 6a)

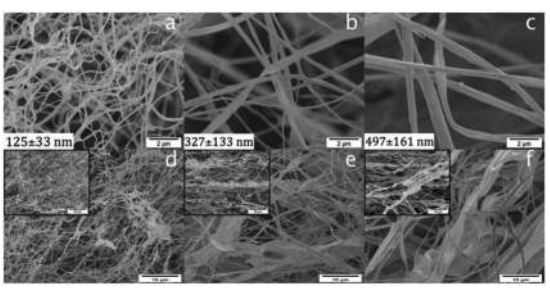

Fig. 6 SEM images of freeze-dried TEMPO oxidized and mechanically defibrillated CNFs: (a,d) CNF1.5; (b,e) CNF3; (c,f) CNF5.

and lengths exceeding hundreds of micrometers (Fig. 6d). These dimensions suggest that the 2–5 nm wide and micrometer long CNF1.5 nanofibrils associate with each other in both lateral and longitudinal directions into super-fine fibers that are larger by more than one magnitude. Similarly ultrafine fibers with average diameter of 153 ($\pm$60) nm have been assembled from mechanically blended CNF at a lower concentration of 0.05 wt%.[29] The dimensional difference in the assembled fibers could be attributed to the different CNF dimensions and concentrations. Although similar in lateral and length dimensions as CNF1.5, CNFs from mechanically blending alone also contain numerous rod-like nanocrystals (100–200 nm in length) which might facilitate CNF assembling into wider fibers. Both freeze-dried CNF3 and CNF5 consisted not only fine fibers (Fig. 6b,c) as CNF1.5 but also broader ribbon-like pieces (Fig. 6e,f), indicating significantly more inter-CNF association. The assembled fibers from CNF3 and CNF5 were averagely 327 ($\pm$133) and 497 ($\pm$161) nm wide, respectively, more than twice and nearly four times wider and also straighter and less wavy than fibers assembled from CNF1.5. The lateral dimensions of CNFs and their self-assembled fibers and solids reflect assembling of hundreds of CNF1.5 nanofibrils to thousands of the thinner and more carboxylated CNF5 nanofibrils. All self-assembled fibers were exceptionally long with lengths exceeding several hundred micrometers (Fig. 6d–f), suggesting assembling of over several hundred nanofibrils in the longitudinal direction.

The fact that much finer and shorter CNF3 and CNF5 assembled into wider fibers than CNF1.5 and even broader ribbon-like pieces may be explained by their smaller dimensions and greater numbers at the same weight concentration as well as their more oxidized surfaces. The finer, more flexible and more numerous CNF3 and CNF5 not only easily entangle but also are more capable of closer packing and inter-nanofibril association. Based on the reduced crystallites dimensions of CNF1.5, CNF3 and CNF5 (eqn (3)), the surface C6 primary hydroxyls were calculated to be 0.268, 0.291 and 0.296 OH/AG, respectively, nearly 4%, 13% and 15% higher than the original rice straw cellulose of 0.257 OH/AG (Table S1 in ESI†). More surface C2 and C3 hydroxyls are also expected from higher specific surfaces of smaller CNFs. Furthermore, C6 carboxyls based on conductometric titration also increased to 0.10, 0.15, and 0.21 COOH/AG, suggesting 38.9%, 58.3% and 81.7% surface C6 primary hydroxyls were converted to carboxyls for CF1.5, CF3 and CF5, respectively. Using their reduced crystallites dimensions, surface C6 carboxyl amounts were slightly lowered to 37.3%, 51.5% and 70.9% for CNF1.5, CNF3 and CNF5, respectively. The greater numbers of surface hydroxyls and the stronger dipoles of surface carboxyl groups of CNF3 and CNF5 equip them with higher hydrogen bonding capacities, enhancing inter nanofibril affinity and resulting larger fibers and more heterogeneous ribbon-like morphologies. The observed self-assembled structures from TEMPO oxidized and mechanically defibrillated CNFs clearly showed that finer CNFs with more numerous hydroxyls and stronger carboxyl dipoles led to more extensive self-assembling into larger fibers and more irregular thin ribbons. Although over 86% of the carboxyls are in sodium salt forms, providing repulsive forces for dispersing CNFs in aqueous media, the much thinner lateral dimensions and more abundant surface C2 and C3 hydroxyls, as well as the residual protonated carboxyls seem to be the dominant factors contributing to their association and self-assembling when concentrated during freeze-drying.

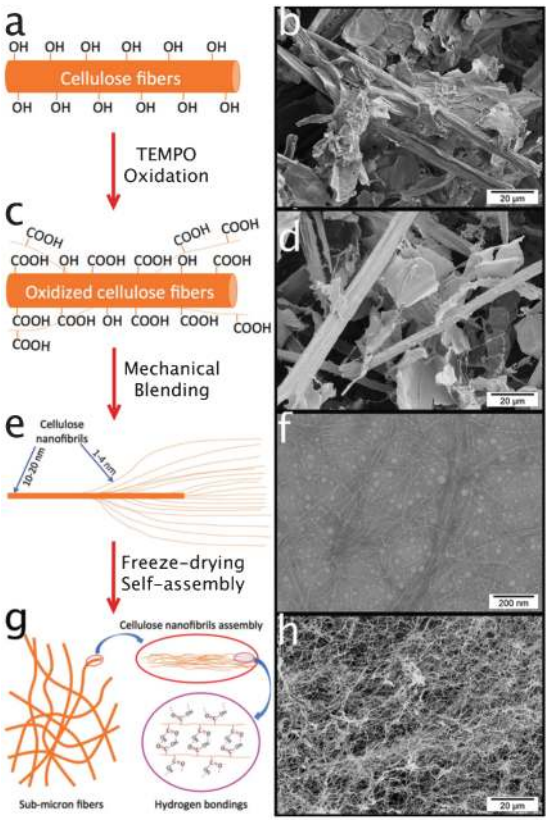

Fig. 7 Defibrillation of rice straw cellulose and self-assembly of cellulose nanofibrils: (a, c, e, g) schematic illustration, not to scale; (b) SEM of pure cellulose; (d) SEM of oxidized CNF1.5; (f) TEM of CNF1.5; (h) SEM of assembled CNF1.5.

TEMPO-mediated oxidation converts the primary C6 hydroxyls in the less ordered regions and on the crystal surfaces of rice straw cellulose into carboxyls (Fig. 7a,c, only the surface hydroxyls and carboxyls were shown). Such oxidation can liberate some nanofibrils by breaking interfibrillar hydrogen bonds and inducing electrostatic repulsions, while most of the oxidized cellulose retained the same macroscopic fiber and fragment morphologies (Fig. 7b,d). Mechanical blending defibrillated the oxidized cellulose macrofibers into partially defibrillated 10–20 nm wide CNFs as well as individual 1–4 nm wide CNFs, all suspended in aqueous media by the electrostatic repulsion of the ionized surface carboxylates (Fig. 7e,f). Self-assembling of CNFs into macroscopic sub-micron fibers from liquid nitrogen freezing and freeze-drying is attributed to ice crystal templating. Exposure to liquid nitrogen induces rapid freezing of large quantities of free water, forming CNF-free ice crystals and CNF-rich domains with concentrated cellulose nanofibrils and CNF surface bound water. During freeze-drying, ice crystals sublimate while the bound water on CNF surfaces evaporates slowly, allowing time for hundreds or

thousands of nanometer wide CNFs to associate in both lateral and longitudinal directions *via* their abundant surface hydroxyl and carboxyl groups (Fig. 7g,h). This self-assembling of dilute aqueous CNF suspension into sub-micron sized fibers is similar to the microwires from liquid nitrogen freezing and freeze-drying of aqueous colloidal suspensions of gold nanoparticles[39] and silica/polymer colloids.[40]

Properties of self-assembled fibrous materials

The self-assembled cellulose fibers exhibited the same cellulose Iβ structure as the starting rice straw cellulose, showing characteristic peaks at 2θ = 14.7°, 16.8° and 22.7° assigned to $1\bar{1}0$, 110, and 200 crystallographic planes of the monoclinic cellulose Iβ lattice, respectively (Fig. 8a). The crystallinity index (CrI) of self-assembled CNF1.5 and CNF3 were 70.8% and 71.5%, similar to the starting cellulose (72.2%), but decreased significantly to 63.2% for self-assembled CNF5, reflecting the more defibrillated and oxidized CNF5 surfaces. FTIR spectra of freeze-dried CNFs showed the same cellulose characteristic peaks as rice straw cellulose, *i.e.*, O–H, C–H and C–O stretching vibration at 3400 cm^{-1}, 2900 cm^{-1} and 1060 cm^{-1}, respectively (Fig. 8b). More importantly, the small shoulders at 3270 and 710 cm^{-1}, characteristic of OH stretching and out-of-plane bending of cellulose Iβ, respectively,[27,41] and the absence of OH stretching and out-of-plane bending at 3240 and 750 cm^{-1} characteristic of cellulose Iα further confirm the cellulose Iβ structure. The peak at 1640 cm^{-1} associated with the O–H bending vibration of absorbed water was evident in spectra of pure cellulose (Fig. 8b), whereas CNF1.5, CNF3 and CNF5 showed a sharp peak at 1612 cm^{-1}, possibly from the overlapping asymmetrical stretching vibrations of carboxylate COO^- in the sodium salt form at 1610 cm^{-1} and the bending vibration of OH of the absorbed water. The small shoulders on CNF1.5, CNF3 and CNF5 at 1710 cm^{-1} associated with the carbonyl stretching (C=O) of the carboxylic acid, suggesting a small portion of the carboxyl groups are in the acid form, consistent with the conductometric titration results. Essentially, conversion of crystalline surface hydroxyl groups to carboxyl groups during TEMPO oxidation was evident from the FTIR, while the core remained in cellulose Iβ structure.

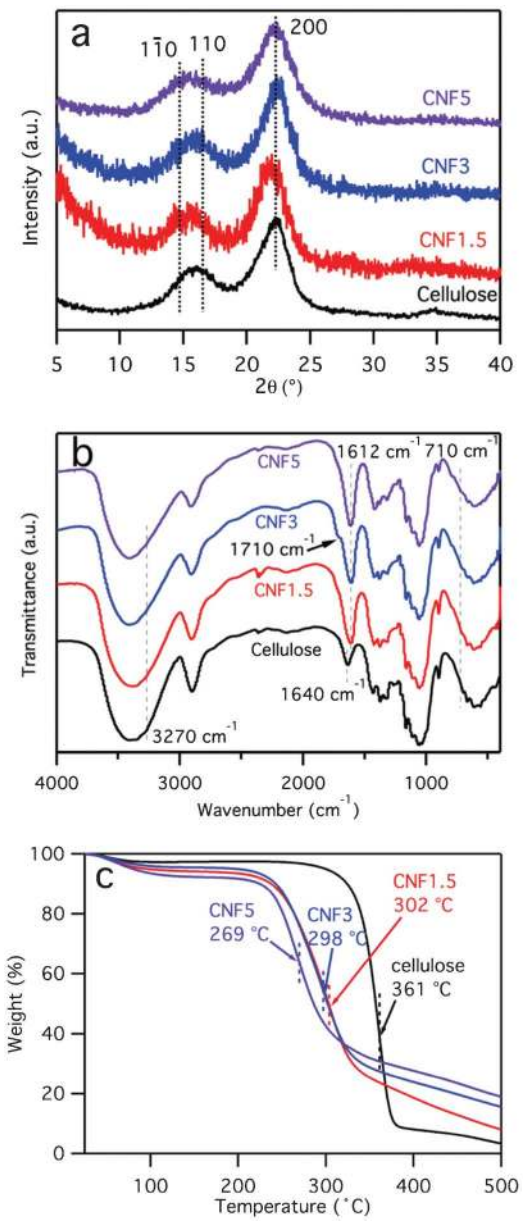

Fig. 8 (a) X-ray diffractogram, (b) FTIR spectrum and (c) TGA of rice straw cellulose (black), self-assembled CNF1.5 (red), CNF3 (blue) and CNF5 (purple).

The TGA of the self-assembled CNFs showed small initial mass loss around 100 °C from evaporation of adsorbed moisture, followed by the most significant mass loss due to decomposition then final mass loss from charring (Fig. 8c). The moisture contents were 2.7%, 4.2%, 5.2% and 6.9% for rice straw cellulose, CNF1.5, CNF3, and CNF5, respectively, consistent with the increasing surface primary hydroxyl-to-carboxyl conversions and the more polar carboxyls. The temperature where maximum weight loss occurs, defined as maximum degradation temperatures (T_{max}) (Fig. S5 in ESI†), decreased from 361 °C for rice straw cellulose to 302 °C, 298 °C and 269 °C for CNF1.5, CNF3 and CNF5, respectively, showing decreasing thermal stability with increasing carboxylation. The significantly lowered onset temperatures for mass loss for TEMPO oxidized cellulose may be explained by the direct solid-to-gas phase transitions of the decarboxylation of surface carboxyl groups.[42,43] Interestingly, despite of the reduced thermal stability, char residues at 500 °C were significantly increased from 3.3% to 8.1, 15.6 and 19.0% for CNF1.5, CNF3 and CNF5, respectively. These more than double to nearly five times higher chars than that of the original rice straw cellulose may have to do with the increasing proportions of interfacial CNF interaction in the self-assembled structures from increased specific surfaces and hydrogen bonding among the hydroxyls and carboxyls. Cellulose nanocrystals (CNCs) from sulfuric acid hydrolysis of cotton had an even lower onset decomposition temperature of 180 °C[27] that was ascribed to the lowered activation energy of decomposition from the surface sulfate groups.[25] Although these TEMPO oxidized CNFs did not yield as high of char residues as the 35% from cotton CNCs,[27] the presence and extent of carboxyls must play a role during thermal decomposition, possibly through cross-

linking or direct solid-to-gas transition from decarboxylation of surface carboxyl. These thermal behaviors of nanocellulose is being further investigated.

This rapid liquid nitrogen freezing and slow freeze-drying combination has shown to be efficient and facile in generating unique super-fine fibers of highly crystalline cellulose Iβ structure at much higher quantity superior to electrospinning which only non-crystalline or cellulose II crystalline structure was possible, due to dissolution of cellulose as in regenerated cellulose. Furthermore, the sizes and morphologies of these super-fine fibrous structures could be tuned by controlling the extent of TEMPO mediated oxidation of cellulose.

Conclusions

Cellulose nanofibrils (CNFs) have been robustly defibrillated from rice straw cellulose by systematic coupling of controlled TEMPO-mediated oxidation and mechanical blending. Under the optimal TEMPO oxidation with 5 mmol g^{-1} NaClO/cellulose or 0.81 NaClO/AG and 30 min mechanical blending, 2 nm wide and micrometer long CNFs were produced at a maximal yield of 96.8%. The so derived CNFs contains 1.29 mmol surface carboxyls per g of cellulose or 0.21 COOH/anhydroglucose (AG), representing 70.9% conversion of surface C6 primary hydroxyls to carboxyls. Both surface charges and reaction times increased linearly with primary oxidant NaClO levels in the 0.24 to 0.81 NaClO/AG range, indicating similar accessibility into the amorphous regions and fast oxidation of C6 primary hydroxyls to carboxyls. TEMPO oxidation at lower NaClO primary oxidant levels yielded less CNFs of 60.3% and 84.5% with less uniform morphologies as well as lower surface C6 primary hydroxyl to carboxyl conversion of 37.3% and 51.5% at 1.5 and 3 mmol g^{-1} NaClO/cellulose, respectively. Doubling the oxidant from 0.81 to 1.62 NaClO/AG increased the hydroxyl-to-carboxyl conversion by 30% but took nearly five times longer in reaction time, showing seriously retarded oxidant accessibility. Super-fine fibrous materials were self-assembled from rapid freezing and freeze-drying of dilute CNF aqueous suspensions, showing sub-micrometer wide and hundreds of micrometer long fibers. Most uniform fibers with diameter of 125 nm could be assembled from CNF with 37.3% surface hydroxyls converted to carboxyls, while additional fiber morphologies could be generated by tuning the geometric and surface characteristics of CNFs. The assembled fibrous materials retained highly crystalline (63.2–71.5% CrI) cellulose Iβ structure, showed lower onset decomposition temperatures and pyrolyzed into more than double and nearly five times of chars than the original rice straw cellulose at 500 °C. This robust defibrillation and self-assembling of rice straw nanocellulose into ultra-fine highly crystalline fibers represents a green and superior alternative to other methods, such as electrospinning, to fabricate comparable ultra-fine cellulose fibrous materials, but with unique cellulose Iβ structure and at much larger and scalable quantities. Converting rice straw, a major under-utilized crop residue, into superior nanomaterials presents further advantages of creating novel and high function products while mitigating environmental impact. These uniquely derived highly crystalline, ultra-high specific surface and highly porous interconnecting cellulose fibers have potential in nanocomposites, separation, biomedical applications and beyond.

Acknowledgements

Financial support for this research from the California Rice Research Board (Project RU-9) is greatly appreciated.

Notes and references

1 Y. Habibi, L. A. Lucia and O. J. Rojas, *Chem. Rev.*, 2010, **110**, 3479–3500.
2 C. Somerville, S. Bauer, G. Brininstool, M. Facette, T. Hamann, J. Milne, E. Osborne, A. Paredez, S. Persson, T. Raab, S. Vorwerk and H. Youngs, *Science*, 2004, **306**, 2206–2211.
3 S. Iwamoto, W. H. Kai, A. Isogai and T. Iwata, *Biomacromolecules*, 2009, **10**, 2571–2576.
4 T. Nishino, I. Matsuda and K. Hirao, *Macromolecules*, 2004, **37**, 7683–7687.
5 D. Klemm, F. Kramer, S. Moritz, T. Lindstrom, M. Ankerfors, D. Gray and A. Dorris, *Angew. Chem., Int. Ed.*, 2011, **50**, 5438–5466.
6 N. Lin, J. Huang and A. Dufresne, *Nanoscale*, 2012, **4**, 3274–3294.
7 R. J. Moon, A. Martini, J. Nairn, J. Simonsen and J. Youngblood, *Chem. Soc. Rev.*, 2011, **40**, 3941–3994.
8 S. Beck-Candanedo, M. Roman and D. G. Gray, *Biomacromolecules*, 2005, **6**, 1048–1054.
9 F. Jiang, A. R. Esker and M. Roman, *Langmuir*, 2010, **26**, 17919–17925.
10 S. P. Dong and M. Roman, *J. Am. Chem. Soc.*, 2007, **129**, 13810–13811.
11 T. Saito and A. Isogai, *Biomacromolecules*, 2004, **5**, 1983–1989.
12 Q. Q. Li and S. Renneckar, *Biomacromolecules*, 2011, **12**, 650–659.
13 M. Paakko, M. Ankerfors, H. Kosonen, A. Nykanen, S. Ahola, M. Osterberg, J. Ruokolainen, J. Laine, P. T. Larsson, O. Ikkala and T. Lindstrom, *Biomacromolecules*, 2007, **8**, 1934–1941.
14 A. Dufresne, J. Y. Cavaille and M. R. Vignon, *J. Appl. Polym. Sci.*, 1997, **64**, 1185–1194.
15 K. Uetani and H. Yano, *Biomacromolecules*, 2011, **12**, 348–353.
16 X. M. Dong, J.-F. Revol and D. G. Gray, *Cellulose*, 1998, **5**, 19–32.
17 P. Lu and Y. L. Hsieh, *Carbohydr. Polym.*, 2012, **87**, 564–573.
18 D. Bondeson, A. Mathew and K. Oksman, *Cellulose*, 2006, **13**, 171–180.
19 A. Isogai, T. Saito and H. Fukuzumi, *Nanoscale*, 2011, **3**, 71–85.
20 T. Saito, Y. Okita, T. T. Nge, J. Sugiyama and A. Isogai, *Carbohydr. Polym.*, 2006, **65**, 435–440.

21 T. Saito, Y. Nishiyama, J. L. Putaux, M. Vignon and A. Isogai, *Biomacromolecules*, 2006, **7**, 1687–1691.
22 T. Saito, S. Kimura, Y. Nishiyama and A. Isogai, *Biomacromolecules*, 2007, **8**, 2485–2491.
23 T. Saito, M. Hirota, N. Tamura, S. Kimura, H. Fukuzumi, L. Heux and A. Isogai, *Biomacromolecules*, 2009, **10**, 1992–1996.
24 R. Zuluaga, J. L. Putaux, J. Cruz, J. Velez, I. Mondragon and P. Ganan, *Carbohydr. Polym.*, 2009, **76**, 51–59.
25 M. Roman and W. T. Winter, *Biomacromolecules*, 2004, **5**, 1671–1677.
26 S. Elazzouzi-Hafraoui, Y. Nishiyama, J. L. Putaux, L. Heux, F. Dubreuil and C. Rochas, *Biomacromolecules*, 2008, **9**, 57–65.
27 P. Lu and Y. L. Hsieh, *Carbohydr. Polym.*, 2010, **82**, 329–336.
28 K. Abe and H. Yano, *Cellulose*, 2009, **16**, 1017–1023.
29 F. Jiang and Y.-L. Hsieh, *Carbohydr. Polym.*, 2013, **95**, 32–40.
30 R. K. Johnson, A. Zink-Sharp, S. H. Renneckar and W. G. Glasser, *Cellulose*, 2009, **16**, 227–238.
31 K. Uetani and H. Yano, *Langmuir*, 2012, **28**, 818–827.
32 L. Segal, J. J. Creely, A. E. Martin Jr and C. M. Conrad, *Text. Res. J.*, 1959, **29**, 786–794.
33 P. Scherrer, *Nachrichten von der Gesellschaft der Wissenschaften zu Göttingen*, 1918, 96–100.
34 Y. Okita, T. Saito and A. Isogai, *Biomacromolecules*, 2010, **11**, 1696–1700.
35 Y. Nishiyama, P. Langan and H. Chanzy, *J. Am. Chem. Soc.*, 2002, **124**, 9074–9082.
36 X. H. Qian, S. Y. Ding, M. R. Nimlos, D. K. Johnson and M. E. Himmel, *Macromolecules*, 2005, **38**, 10580–10589.
37 R. Shinoda, T. Saito, Y. Okita and A. Isogai, *Biomacromolecules*, 2012, **13**, 842–849.
38 Q. Li and S. Renneckar, *Cellulose*, 2009, **16**, 1025–1032.
39 H. Zhang, J. Y. Lee, A. Ahmed, I. Hussain and A. I. Cooper, *Angew. Chem., Int. Ed.*, 2008, **47**, 4573–4576.
40 Q. H. Shi, Z. S. An, C. K. Tsung, H. J. Liang, N. F. Zheng, C. J. Hawker and G. D. Stucky, *Adv. Mater.*, 2007, **19**, 4539–4543.
41 M. Wada, T. Kondo and T. Okano, *Polym. J.*, 2003, **35**, 155–159.
42 H. Fukuzumi, T. Saito, Y. Okita and A. Isogai, *Polym. Degrad. Stab.*, 2010, **95**, 1502–1508.
43 H. Fukuzumi, T. Saito, T. Wata, Y. Kumamoto and A. Isogai, *Biomacromolecules*, 2009, **10**, 162–165.